Acta Crystallographica Section B
Structural Science
ISSN 0108-7681

The mapping of electronic energy distributions using experimental electron density

Vladimir G. Tsirelson

Mendeleev University of Chemical Technology, Miusskaya Sq. 9, Moscow 125047, Russia

Correspondence e-mail: tsirel@muctr.edu.ru

Received 26 December 2001
Accepted 25 March 2002

It is demonstrated that the approximate kinetic energy density calculated using the second-order gradient expansion with parameters of the multipole model fitted to experimental structure factors reproduces the main features of this quantity in a molecular or crystal position space. The use of the local virial theorem provides an appropriate derivation of approximate potential energy density and electronic energy density from the experimental (model) electron density and its derivatives. Consideration of these functions is not restricted by the critical points in the electron density and provides a comprehensive characterization of bonding in molecules and crystals.

1. Introduction

Electron density $\rho(\mathbf{r})$, its gradient vector field $\nabla\rho(\mathbf{r})$, its Laplacian $\nabla^2\rho(\mathbf{r})$ field and characteristics of the critical points [the points where $\nabla\rho(\mathbf{r}) = 0$] provide a quantitative description of bonding in molecules and crystals in terms of quantum-mechanical topological theory (Bader, 1990). The pairs of gradient lines in the $\nabla\rho(\mathbf{r})$ field originated at the saddle critical point between atoms, $\mathbf{r}_b$, and terminated at two neighboring nuclei, along which the electron density (ED) is maximal with respect to any other line, are the most important for characterization of the atomic interactions. They form the atomic interaction lines named the bond paths in an equilibrium system. Corresponding bond critical points are denoted as (3,−1): they are characterized by three non-zero eigenvalues of the curvature or Hessian matrix, λ_i, and the sum of the algebraic signs of λ_i is −1. Values $\lambda_1 < 0$ and $\lambda_2 < 0$ measure the degree of the ED contraction towards the bond critical point, while $\lambda_3 > 0$ measures the degree of the ED contraction towards each of the bonded nuclei. The sign of the Laplacian at the bond critical point $\nabla^2\rho(\mathbf{r}_b) = \lambda_1 + \lambda_2 + \lambda_3$ depends on the relationship between the λ_i values at this point. If the electrons are locally concentrated around the bond critical point [$\nabla^2\rho(\mathbf{r}_b) < 0$], the electrons are shared by both nuclei: this is typical for shared or covalent atomic interactions. Otherwise the electrons are concentrated in each of the atomic basins [$\nabla^2\rho(\mathbf{r}_b) > 0$] and the atomic interaction belongs to the closed-shell type. The latter is typical for ionic, hydrogen and van der Waals bonds (Bader & Essen, 1984; Bone & Bader, 1996). Thus, $\nabla^2\rho(\mathbf{r}_b)$ reflects the character of the atomic interactions.

Local concentrations and depletions of the electrons in the internuclear space are connected with the features of the electronic energy distribution *via* the local form of the virial theorem (Bader & Beddall, 1972):

$$2g(\mathbf{r}) + v(\mathbf{r}) = (\hbar^2/4m)\nabla^2\rho(\mathbf{r}). \quad (1)$$

The latter expression gives an exact explicit relationship between the second derivative of the electron density and the (quasi-classical) electronic kinetic energy density

$$g(\mathbf{r}) = (\hbar^2/2m)\nabla_{\mathbf{r}}\nabla_{\mathbf{r}'}\gamma(\mathbf{r}, \mathbf{r}')_{\mathbf{r}=\mathbf{r}'} \quad (2)$$

and electronic potential energy density

$$v(\mathbf{r}) = -\sum_a \left[Z_a e^2/(\mathbf{r} - \mathbf{R}_a)\right]\rho(\mathbf{r}) + e^2 \int \left[\Gamma(\mathbf{r}, \mathbf{r}_1)/(\mathbf{r} - \mathbf{r}_1)\right] \mathrm{d}\mathbf{r}_1. \quad (3)$$

Here, $\gamma(\mathbf{r}, \mathbf{r}')$ and $\Gamma(\mathbf{r}, \mathbf{r}_1)$ are one- and two-electron density matrices, respectively, Z_a is the charge of nucleus a, e is the electron charge, and m is the electron mass. One-electron functions $g(\mathbf{r})$ and $v(\mathbf{r})$ describe the local contributions to the electronic kinetic and potential energies; $g(\mathbf{r}) > 0$ and $v(\mathbf{r}) < 0$ everywhere in the equilibrium system (Bader & Essen, 1984; Bader, 1998). The local electronic potential energy dominates at the (3,−1) critical point in the case of the shared-type atomic interactions. Whether kinetic or potential electronic energy will locally dominate in the closed-shell bond critical point depends on the specificity of the bonding.

The density of the electronic energy (Bader & Beddall, 1972)

$$h_e(\mathbf{r}) = g(\mathbf{r}) + v(\mathbf{r}) \quad (4)$$

gives a more straightforward criterion for the recognition of the atomic interaction type: $h_e(\mathbf{r}_b) < 0$ is observed in shared-type atomic interactions, while $h_e(\mathbf{r}_b) > 0$ is observed in closed-shell interactions (Cramer & Kraka, 1984; Bone & Bader, 1996).

The electronic potential density distribution represents the virial field of the Ehrenfest (1927) force acting on an electron at $\mathbf{r}$ (Bader, 1994, 1998). The Ehrenfest force governs the motion of electrons and, therefore, plays an important role in the quantum mechanics of molecules and crystals (Bader, 1994). Keith *et al.* (1996) noted that for every atomic interaction type, each bond path is homeomorphically mirrored by a virial path, a line of maximally negative potential energy density linking the same nuclei. According to Bader (1998), the presence of the virial path provides an indicator of bonding atomic interaction. The network of virial and bond paths linking neighboring nuclei defines a molecular graph, which is invariant to the nuclear vibrations in a stable system.

Thus, consideration of the local electronic energies provides a direct approach to characterization of bonding in molecules and crystals. Bader & Preston (1969), Bader & Beddall (1972), Keith *et al.* (1996) and Bader (1998) have studied energy distributions in molecules; their calculations were based on wave functions. On the other hand, the electronic kinetic energy density $g(\mathbf{r})$ can be calculated within the density functional formalism, which allows the avoidance of any wave-function calculation (Hohenberg & Kohn, 1964; Kirzhnits *et al.*, 1975; Lundqvist & March, 1983; Dahl & Avery, 1984; Dreizler & Gross, 1990; Ellis, 1995; Springborg, 1997). Tsirelson (1992) pointed out that combining the density functional theory and ED derived from X-ray diffraction significantly expands the frameworks of the traditional structure analysis. In this work, this approach will be explored and results will be presented for the local energy functions obtained for crystals with different types of chemical bonds.

The local energy functions can also be calculated using the one-electron density matrix reconstructed from the electron density (Tsirelson *et al.*, 1977; Tsirelson & Ozerov, 1979, 1996; Clinton *et al.*, 1983; Gritsenko & Zhidomirov, 1987; Levy & Goldstein, 1987; Aleksandrov *et al.*, 1989; Schwarz & Mueller, 1990; Schmider *et al.*, 1992; Zhao & Parr, 1993; Jayatilaka, 1998). This approach is not discussed here.

2. Functionals for kinetic energy

The main problem in density functional theory consists in expressing the kinetic, exchange and correlation energy densities in terms of $\rho(\mathbf{r})$ (Lundqvist & March, 1983; Parr & Yang, 1989; Dreizler & Gross, 1990; Reznik, 1992; Tsirelson & Ozerov, 1996). The standard way to solve this problem for kinetic energy density uses the fact that the one-electron density matrix $\gamma(\mathbf{r}, \mathbf{r}')$ is related to the one-particle Green function by the inverse Laplace transform (Parr & Yang, 1989). Both gradient $\hbar$-expansion of the Green function around the classical Thomas–Fermi approximation (Kirzhnits, 1957) and presentation of the zero-order Green function in the mean-path approximation using the Feynman path-integral method (Yang, 1986) lead to the same general expression for kinetic energy density:

$$g(\mathbf{r}) = \left(\frac{3\hbar^2}{10m}\right)(3\pi^2)^{2/3}\rho(\mathbf{r})^{5/3} + \frac{\lambda(\hbar^2/m)\left[\nabla\rho(\mathbf{r})\right]^2}{\rho(\mathbf{r})} + k\left(\frac{\hbar^2}{2m}\right)\nabla^2\rho(\mathbf{r}). \quad (5)$$

The gradient expansion, which is valid for smooth (but not necessary small) variations of the electron density, gives $\lambda = 1/72$ and $k = 1/6$, while the mean-path approximation leads to $\lambda = 1/72$ and $k = 1/12$. Weizsaecker (1935), taking one-electron wave functions as the modified plane waves, arrived at equation (5) with $\lambda = 1/8$ and $k = 0$: his result, corresponding to a fast-oscillating ED, does not follow, however, from either gradient expansion or mean-path approximation.

Kirzhnits (1957), Santos & Villagra (1972), Kirzhnits *et al.* (1975), Brack *et al.* (1976), Alonso & Girifalco (1978), Grammaticos & Voros (1979), Yang (1986), Yang *et al.* (1986), Dreizler & Gross (1990), Yang *et al.* (1996), Abramov (1997*a*) and Fuentealba (1997) stressed the importance of the Laplacian term in equation (5). The latter does not affect the average energy of a system, but it provides a description of the electronic shells and improves the local kinetic energy behavior in the valence electron areas.

Consideration of the asymptotic behavior of the kinetic energy density (2) derived from the one-electron density matrix (Bader & Beddall, 1972) shows that $g(\mathbf{r})$ goes to $\frac{1}{2}Z^2\rho_i(\mathbf{R}_i)$ with $\mathbf{r} \Rightarrow \mathbf{R}_i$, where $\rho_i(\mathbf{R}_i)$ is the value of the ED at nucleus positions $\mathbf{R}_i$. From (5), the approximate value of $g(\mathbf{r})$

goes to minus infinity with $\mathbf{r} \Rightarrow \mathbf{R}_i$ because of the Laplacian term. Therefore, the regions close to the nuclei should be excluded from consideration during the interpretation of the approximate $g(\mathbf{r})$. Note that the accuracy of determination of both experimental and theoretical electron densities and their derivatives near nuclei is pure owing to a variety of factors discussed by Tsirelson & Ozerov (1996). The long-range behavior of the approximate $g(\mathbf{r})$ is physically acceptable provided expansion is restricted by the second-order term (Tal & Bader, 1978).

The size of the holes around the nuclei within which an approximate g becomes negative is quite small. For example, for gradient expansion, the hole radius is maximal for hydrogen atoms (0.15 Å); it is less than 0.02 Å for atoms with $Z \geq 11$ and reaches a value of 0.005 Å for $Z = 36$. This observation fits the $1/Z$-dependency for the hole radius marked by Yang *et al.* (1986). Thus, the region where the approximation (5) is not suitable for describing the kinetic energy density is completely within the area of uncertainty (due to experimental and model errors in ED) of this function.

It is well documented (Politzer & Parr, 1974; Tal & Bader, 1978; Parr & Yang, 1989; Reznik, 1992) that the average molecular energy calculated by the variational principle using expression (5) is only qualitatively close to the experimental one. At the same time, the use of the Hartree–Fock wave functions to describe ρ in (5) results in the average kinetic energy differing from the Hartree–Fock value by about 1%. The accuracy of the model electron density reconstructed from X-ray diffraction experiments is the same order as the Hartree–Fock electron density provided the regions close to the nuclei are excluded from consideration (Tsirelson & Ozerov, 1996). This quasi-static ED obtained by the fit of some analytical structural model to the measured intensities corrected for multiple scattering, absorption, thermal diffuse scattering and extinction is only slightly distorted by experimental and model errors (Tsirelson & Ozerov, 1996). It is also close to the quantum-mechanical ρ calculated using wave functions obtained by the variational principle. Significantly, the model ED exhibits the same set of critical points as the quantum-mechanical ρ (Kapphahn, Tsirelson & Ozerov, 1988, 1989; Tsirelson *et al.*, 1998), and it can be considered to be a homeomorphic image of the 'true' ρ derived from first principles.

Following Masunov & Vyboishchikov (1993), Abramov (1997*a*) studied the kinetic energy values at the bond critical points using expression (5) with $\lambda = 1/72$ and $k = 1/6$ (gradient expansion) and experimental ED in some covalent and ionic compounds. Espinosa *et al.* (1998, 1999) and Espinosa & Molins (2000) applied the same approach to the determination of the energy characteristics of the hydrogen bonds in a number of crystalline systems. The local potential energy $v(\mathbf{r})$ and electronic energy $h_e(\mathbf{r})$ at the bond critical points were determined using expressions (1), (4) and (5). However, it is appropriate to mention here that the model ED is derived by the fit to experimental structure factors, not by the variational principle. Hence, it does not necessarily obey the local virial theorem (1) and can lead to unphysical potential energy distributions. Therefore, firstly, it is essential to clarify to what extent this approach is suitable for the determination of the local energy characteristics.

To explore this point, we calculated the kinetic energy density (5) for crystalline LiF using quantum-mechanically valid Hartree–Fock electron densities. In accord with Bader & Platts (1997), a cubic-like cluster $Li_{14}F_{13}^{+}$ surrounding the central fluorine ion was used to simulate an LiF crystal. The PC version (Granovsky, 2000) of program *GAMESS* (Schmidt *et al.*, 1993) was used. The wave function for LiF was calculated in the 6–311 G* basis set; the optimized geometry of a cluster was taken from Bader & Platts (1997). Then, both the gradient expansion (Kirzhnits, 1957) and mean-path (Yang, 1986) approximations were used to calculate the kinetic energy density $g(\mathbf{r})$ (5). The local potential energy $v(\mathbf{r})$ was calculated using the local virial theorem (1), which is valid in the Hartree–Fock theory. Functions $g(\mathbf{r})$ (2) and $v(\mathbf{r})$ (3) were also calculated directly from the Hartree–Fock wave functions using the *AIMPAC* program suite (Biegler-Koenig *et al.*, 1982).

A comparison of the approximate local energy densities with the Hartree–Fock ones for the crystalline LiF is given in Figs. 1 and 2. These figures show that the kinetic energy densities calculated using the gradient expansion and mean-path approximation differ in the low electron density regions at the center of the (100) plane. This difference has an important consequence: the function $g(\mathbf{r})$ calculated using the Kirzhnits (1957) gradient expansion leads to the potential energy density, which is negative everywhere, while the Yang (1986) approximation results in physically unacceptable positive regions in the local potential energy corresponding to the low electron density regions.

We performed similar calculations for some crystals with rock-salt structure (Tsirelson & Ivanov, 2000), diamond and solid krypton (Tsirelson, 2000), and single molecules of LiF and urea, $CO(NH_2)_2$, and obtained the same result: the Yang (1986) approximation led to positive areas in the local potential energy corresponding to low electron density regions (such regions, for example, are to be found on the periphery of free molecules).

According to Yang *et al.* (1986), the mean-path approximation provides a better zero-order description for both diagonal and off-diagonal elements of the one-electron density matrix, at least at the Wentzel–Kramers–Brillouin (WKB) approximation level. However, the positive areas in the potential energy density, calculated from the Hartree–Fock electron density using Yang's approximation for the kinetic energy and the local virial theorem (1), led us to conclude that the Kirzhnits (1957) approximation (or gradient expansion) is preferable for studying the energy distributions. Moreover, the Kirzhnits (1957) kinetic energy density g($\mathbf{r}$) is closer to the Hartree–Fock one (Fig. 1). For this reason, the kinetic energy densities discussed in the rest of this work were obtained by the gradient expansion method only. The energy density functions calculated from the Hartree–Fock ED using this approximation will be referred to henceforth as HF/DFT ones, while functions calculated using the model ED derived

Table 1
The characteristics of the (3,−1) bond critical point in an LiF crystal (a.u.).

Interaction	Origin of the electron density	$\rho(\mathbf{r}_b)$	$\nabla^2\rho(\mathbf{r}_b)$	$v(\mathbf{r}_b)$	$g(\mathbf{r}_b)$	$h_e(\mathbf{r}_b)$
Li−F	Hartree–Fock	0.022	0.183	−0.029	0.038	0.009
	Experiment	0.021 (2)	0.156 (1)	−0.021 (2)	0.032 (2)	0.011 (2)
	Ionic procrystal	0.019	0.156	−0.022	0.030	0.008
F−F	Hartree–Fock	0.013	0.052	−0.0127	0.0128	0.0001
	Experiment	0.012 (1)	0.041 (2)	−0.007 (2)	0.009 (2)	0.002 (2)
	Ionic procrystal	0.012	0.042	−0.008	0.008	0.000

Table 2
The characteristics of the (3,−1) critical points in a single urea molecule.

The experimental and Hartree–Fock values are presented in the first and second lines, respectively.

Bond	Bond distance (Å)	$\rho(\mathbf{r}_b)$ (e Å^{-3})	$\nabla^2\rho(\mathbf{r}_b)$ (e Å^{-5})	$g(\mathbf{r}_b)$ (a.u.)	$v(\mathbf{r}_b)$ (a.u.)	$h_e(\mathbf{r}_b)$ (a.u.)
C−O	1.258 (1)	2.25 (5)	−23.69 (20)	0.398	−1.050	−0.652
	1.195†	2.95	−24.425	0.730	−1.505	−0.776
C−N	1.343 (1)	2.34 (5)	−32.32 (23)	0.272	−0.871	−0.599
	1.362	2.19	−22.227	0.268	−0.767	−0.499
N−H$_1$ (N−H$_2$)‡	1.001 (4)	2.01 (5)	−42.06 (30)	0.088	−0.614	−0.526
	0.991	2.41	−47.139	0.054	−0.597	−0.543

† Molecular geometry optimization was performed in the 6–311 G** basis set. Values of the optimized valence angles are C−N−H1 117.24°, C−N−H2 123.50°, N−C−O 122.57°. ‡ Experimental intramolecular N−H distances and corresponding characteristics of the (3,−1) critical points, which are different in a crystal, were averaged.

from X-ray diffraction experiments will be denoted as EXP/DFT.

Compare now the $g_{EXP/DFT}$ and $v_{EXP/DFT}$ functions calculated using the experimentally derived parameters of the multipole model for an LiF crystal (Tsirelson *et al.*, 1998) and a single (removed from a crystal) molecule of urea (Zavodnik *et al.*, 1999) with the Hartree–Fock ones. Corresponding maps are presented in Figs. 3 and 4, while numerical characteristics of these functions are listed in Tables 1 and 2. Optimization of geometry and calculation of the wave function for a free urea molecule was done in the 6–311 G** basis set; the results were very close to those of Gatti *et al.* (1994). The periphery of the model electron density of a urea molecule removed from a crystal is slightly perturbed by the intermolecular interactions (Fig. 4*a*). Moreover, the geometrical parameters of a urea molecule in a crystal differ from those in a free state (Table 2). In spite of that, the same functions obtained from different sources are in reasonable agreement for both LiF and urea. The maximal discrepancy between HF/DFT and EXP/DFT densities g and v (Figs. 3 and 4) is observed in regions very close to the nuclei (which are omitted in the figures) for the reason explained above. The agreement of the (3,−1) critical point characteristics (Tables 1 and 2) for both functions could be appraised as semi-quantitative. We can hardly expect a better agreement. First, the rapid variation of the electron density in the vicinity of the nuclei and its slow variation in the valence electron shells prevents the existence of the density functional approximation for $g(\mathbf{r})$, which provides a good description everywhere in the position space (Tal & Bader, 1978; Parr & Yang, 1989; Reznik, 1992). Second, the leading term in the kinetic energy density expansion (5) comes from the statistical Thomas–Fermi theory, which is valid for high-density regions. Quantum corrections improve the local behavior of this function; however, discrepancy with the Hartree–Fock kinetic energy density still remains. At the same

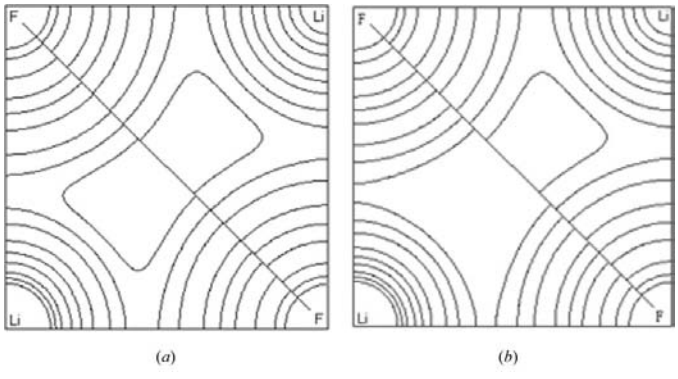

Figure 1
Distributions of the kinetic energy $g(\mathbf{r})$ in the (100) plane of crystalline LiF. The upper-right triangle represents the $g(\mathbf{r})$ function calculated directly from the Hartree–Fock wave functions by expression (2), while the lower-left triangle represents the $g(\mathbf{r})$ function calculated using the Hartree–Fock electron density by expression (5) with (*a*) $\lambda = 1/72$ and $k = 1/6$ [Kirzhnits (1957) approximation] and (*b*) $\lambda = 72$ and $k = 1/12$ [Yang (1986) approximation]. Line intervals are 2×10^n a.u., 4×10^n a.u. and 8×10^n a.u. ($-2 \le n \le 1$).

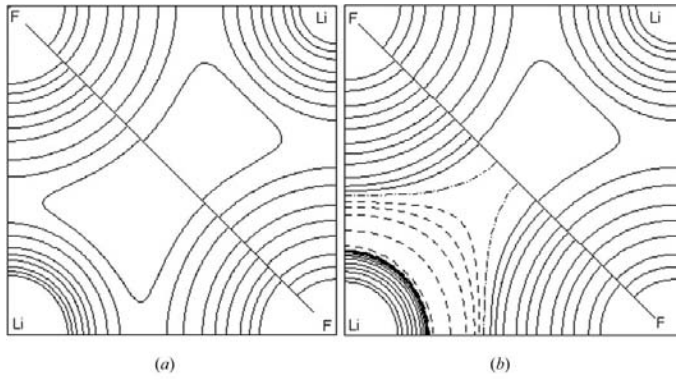

Figure 2
Distributions of the potential energy $v(\mathbf{r})$ in the (100) plane of crystalline LiF. The upper-right triangle represents the $v(\mathbf{r})$ function calculated directly from the Hartree–Fock wave functions by expression (3), while the lower-left triangle represents the $v(\mathbf{r})$ function calculated using the Hartree–Fock electron density by combination of expressions (1) and (5) with (*a*) $\lambda = 1/72$ and $k = 1/6$ [Kirzhnits (1957) approximation] and (*b*) $\lambda = 1/72$ and $k = 1/12$ [Yang (1986) approximation]. Line intervals are $\pm 2 \times 10^n$ a.u., $\pm 4 \times 10^n$ a.u. and $\pm 8 \times 10^n$ a.u. ($-2 \le n \le 1$). Negative values are solid, zero contour is dot-dashed.

time, it is essential that the local energy functions $g_{\rm EXP/DFT}$ and $v_{\rm EXP/DFT}$ exhibit the same topology as the appropriate Hartree–Fock functions. The only exception is the N$\cdots$H bond, where the negative hole in $g_{\rm EXP/DFT}$, mentioned above, devours the saddle points in $g_{\rm EXP/DFT}$ and $v_{\rm EXP/DFT}$.

Thus, approximation of the kinetic energy density by the gradient expansion and its calculation using parameters of the multipole model fitted to experimental structure factors reasonably reproduces the main features of this quantity in a position space of a molecule or crystal. The use of the local virial theorem also provides the appropriate derivation of the approximate potential energy density from the model ED. We can conclude that combination of the formulae of the density functional theory and the model electron density is proved to be useful for characterization of bonding in molecules and crystals in terms of the local energy functions.

3. The features of the local energy functions for closed-shell and shared-type atomic interactions

Consider now the features of the local energy functions obtained from the model electron density for crystalline LiF and urea – compounds with different types of interatomic interactions.

The distributions of the local kinetic energy, $g_{\rm EXP/DFT}(\mathbf{r})$, and potential energy, $v_{\rm EXP/DFT}(\mathbf{r})$, and the density of the electronic energy, $h_{\rm e,EXP/DFT}(\mathbf{r})$, in LiF are shown in Fig. 5. The values of these functions in the (3,−1) critical points in the ED are given in Table 1. First, note that the function $-v$ is structurally homeomorphic to the ED depicted in Fig. 3(*a*). This means that each virial path in $-v$ will mirror a bond path in the electron density of the crystalline LiF as observed by Keith *et al.* (1996) for molecules. Second, the network of the bond and virial paths (they are not shown in the figures)

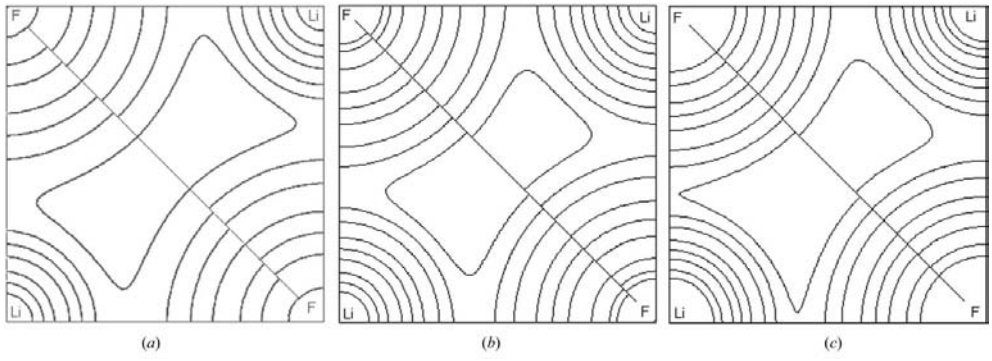

Figure 3
Distributions of the electron density (*a*) and the kinetic (*b*) and potential (*c*) energies in the (100) plane of crystalline LiF. The upper-right triangle represents the functions calculated directly from the Hartree–Fock wave functions, while the lower-left triangle represents the functions calculated, as explained in the text, using the model electron density deduced from X-ray diffraction experiments. The Kirzhnits (1957) approximation was used to calculate the kinetic energy density. Line intervals are 2×10^n a.u., 4×10^n a.u. and 8×10^n a.u. for (*a*) ($-2 \le n \le 0$) and (*b*) ($-2 \le n \le 1$), and (*c*) -2×10^n a.u., -4×10^n a.u. and -8×10^n a.u. for ($-2 \le n \le 1$).

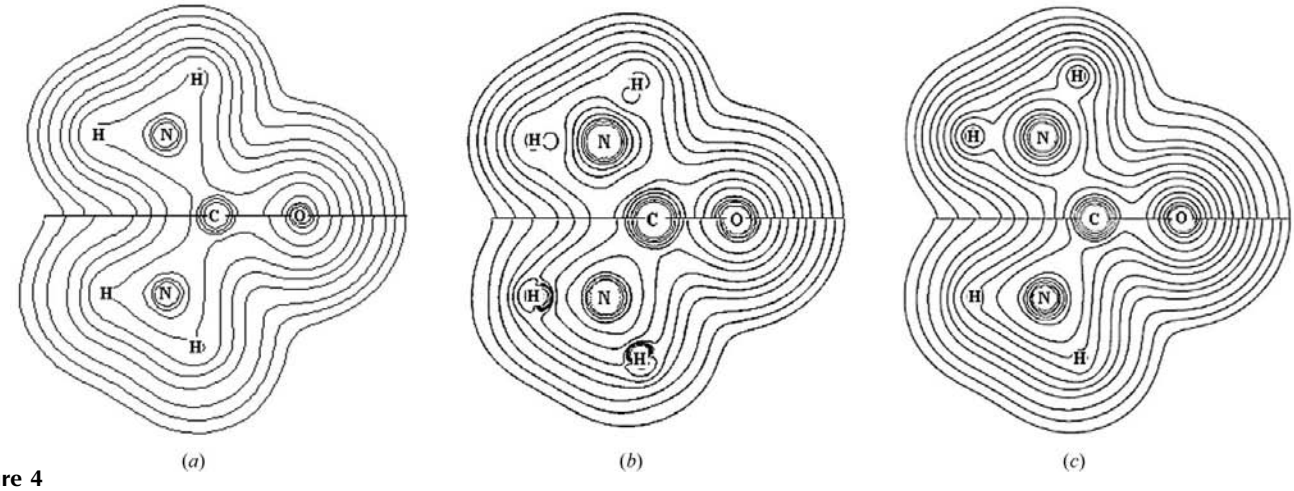

Figure 4
Distributions of the electron density (*a*) and the kinetic (*b*) and potential (*c*) energies in a single (removed from a crystal) urea molecule. The upper part of the picture represents the functions calculated directly from the Hartree–Fock wave functions, while the lower triangle represents the functions calculated, as explained in the text, using the multipole parameters of the electron density derived from X-ray diffraction experiments. The Kirzhnits (1957) approximation was used to calculate the kinetic energy density. Line intervals are 2×10^n a.u., 4×10^n a.u. and 8×10^n a.u. ($-2 \le n \le 2$); solid lines correspond to negative values of the potential energy density. The geometrical parameters of a free molecule and a molecule in a crystal are different (see Table 2). For this reason, the maps were merged so that the positions of the C atoms coincided.

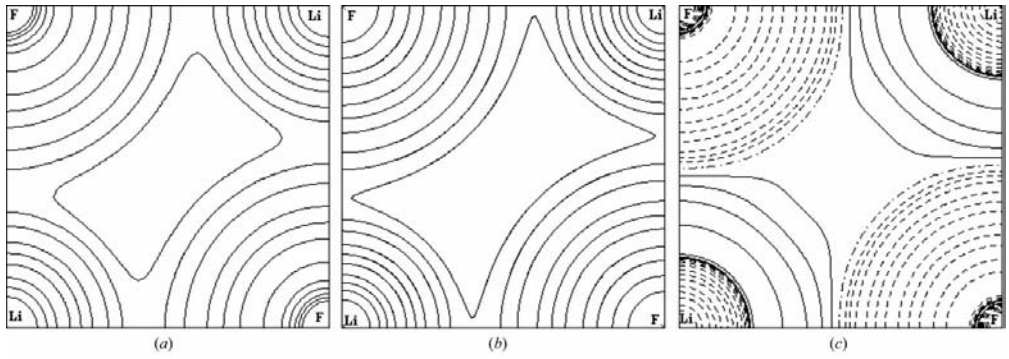

Figure 5
Distributions of the kinetic (*a*), potential (*b*) and electronic (*c*) energies in the (100) plane of crystalline LiF calculated using the model electron density derived from X-ray diffraction experiments and formulae of the density functional theory (see text). Line intervals are (*a*) 2×10^n a.u., 4×10^n a.u. and 8×10^n a.u. ($-2 \le n \le 0$); (*b*) -2×10^n a.u., -4×10^n a.u. and -8×10^n a.u. ($-2 \le n \le 2$); (*c*) $\pm 2 \times 10^n$ a.u., $\pm 4 \times 10^n$ a.u. and $\pm 8 \times 10^n$ a.u. ($-2 \le n \le 2$). Solid lines correspond to negative values of the potential energy density and positive values of the electronic energy density in (*b*) and (*c*), respectively.

connects the nearest-neighbor Li–F and F–F atomic pairs. Thus, the secondary atomic interactions in the rock-salt type crystals discussed by Tsirelson (1996), Tsirelson *et al.* (1998), Luana *et al.* (1997), Martin Pendas *et al.* (1998) and Abramov (1997*b*) manifest themselves in the potential energy distribution, not just in the electron density. Finally, the electronic energy density h_e (Fig. 5*c*) has a minimum along these lines, having positive values in (and around) the ED bond critical points.

These observations give a much more complete picture of the closed-shell atomic interactions than is usually obtained in the treatment of experimental electron density in terms of the values of the ED and the Laplacian of the ED at the bond critical points. In particular, Fig. 5(*c*) also explicitly reveals the stabilizing role of the anions in forming the LiF crystal structure. This supports the early conclusion by Martin Pendas *et al.* (1998), based on the features of the Laplacian of the ED in binary ionic crystals. The potential energy is negative along the F—F lines and there is no evidence of any pairwise F—F-specific interactions, as has been suggested (Abramov, 1997*b*). The latter observation is in accordance with the quantum-mechanical explanation of the bonding in LiF given by Bader (1998).

Note that energy characteristics calculated for an ionic procrystal model (a hypothetical set of spherical atoms or ions placed in the same positions as the real ones) in LiF are in very good agreement with the experimental ones (Table 1). From one side, this means that topological analysis of a procrystal may be used for *a priori* prediction of properties of ionic compounds. On the other side, however, we need to make more effort to establish the subtle changes in the electron density and energy characteristics separating a crystal from a procrystal.

The distributions of the same local energy functions in crystalline urea, $CO(NH_2)_2$, are shown in Fig. 6. The structure of this compound [space group $P\bar{4}2_1m$, $Z = 2$ (2 mm)] is characterized by the ribbons of doubly hydrogen-bonded molecules arranged in a head-to-tail fashion along the *c* axis.

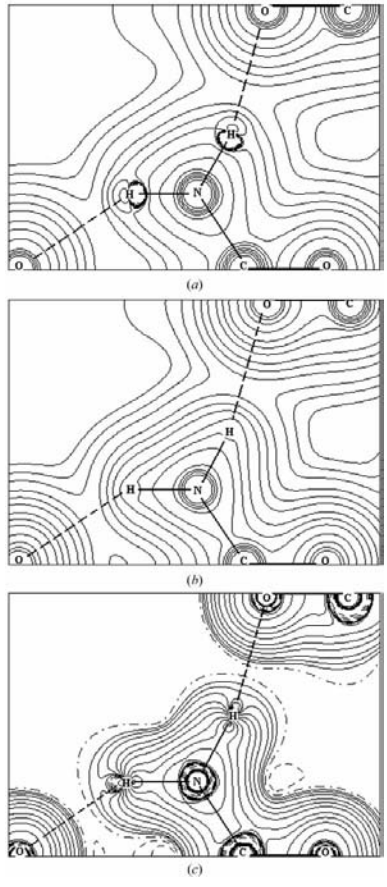

Figure 6
Distributions of the kinetic (*a*), potential (*b*) and electronic (*c*) energies in crystalline urea (half of the molecule is shown) calculated using the model electron density derived from X-ray diffraction experiments and formulae of the density functional theory (see text). Line intervals are (*a*) 2×10^n a.u., 4×10^n a.u. and 8×10^n a.u. ($-3 \le n \le 1$); (*b*) -2×10^n a.u., -4×10^n a.u. and -8×10^n a.u. ($-3 \le n \le 1$); (*c*) $\pm 2 \times 10^n$ a.u., $\pm 4 \times 10^n$ a.u. and $\pm 8 \times 10^n$ a.u. ($-3 \le n \le 1$). Solid lines correspond to negative values of the potential energy density and electronic energy density in (*b*) and (*c*), respectively; dashed lines indicate hydrogen bonds. Small negative areas in the kinetic energy density close to atomic centers are omitted.

The plane of each ribbon is perpendicular to the adjacent ribbons oppositely directed along the *c* axis. The O atom of a carbonyl group in one ribbon is also involved in hydrogen bonds with two adjusted ribbons. We can see that the potential energy density is again homeomorphic to the ED and dominates in all the intramolecular space. Electronic energy density $h_e(\mathbf{r})$ (Fig. 6*c*) is maximally negative along the intramolecular bond lines in urea. It is also strongly negative inside the atomic cores exhibiting the shell structure of bonded atoms. At the same time, it is slightly positive around the ED (3,−1) bond critical points in the hydrogen bonds in urea, where the kinetic energy dominates. This agrees with early observations made for weakly bounded molecular systems (Bone & Bader, 1996) and hydrogen bonds (Espinosa *et al.*, 1999). Note that the longer hydrogen bond [$d_{O\cdots H} = 2.071$ (2) Å] is characterized by a minimal value of $h_{e,min} = +0.00125$ a.u., while the shorter hydrogen bond [$d_{O\cdots H} = 2.014$ (2) Å] has the less positive value $h_{e,min} = +0.00055$ a.u.

To reveal the fine features of the atomic interactions in crystalline urea, we have also calculated the difference functions (Bader & Preston, 1969)

$$\delta g(\mathbf{r}) = g_{cryst}(\mathbf{r}) - g_{procryst}(\mathbf{r}) \quad (6)$$

and

$$\delta v(\mathbf{r}) = v_{cryst}(\mathbf{r}) - v_{procryst}(\mathbf{r}) \quad (7)$$

depicted in Fig. 7. The subscript 'cryst' denotes functions calculated for a crystal, while the subscript 'procryst' denotes functions calculated for a procrystal. Both difference functions exhibit changes in the corresponding energy densities caused by the formation of a urea crystal from the atoms. We can see that kinetic energy is increased strongly in the atomic cores of non-H atoms (areas close to the nuclear positions are omitted), being maximal in the N atom's core, and slightly in the intramolecular bonds and electron lone-pair regions. Potential energy increases strongly in both the atomic cores of non-H atoms and the intramolecular bonds and electron lone-pair regions. The distribution of $\delta g(\mathbf{r})$ on the end O and H atoms has a dipolar character, being positive behind the nuclear positions. The distribution of $\delta v(\mathbf{r})$ also has a dipolar character; however the (negative) potential energy density diminishes behind the H atoms and increases behind the O atom during crystal formation. As a result, the positive electronic energy density $h_e(\mathbf{r})$ dominates behind the H nucleus positions (Fig. 6*c*). This finding may be useful in modeling the hydrogen bond.

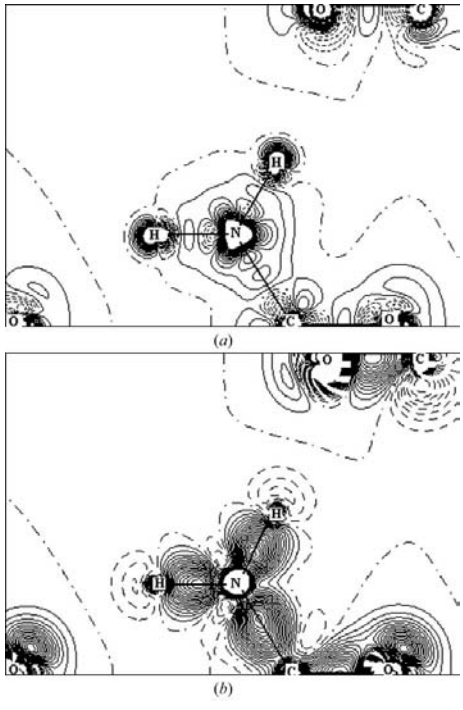

Figure 7
Crystalline urea: the difference functions $\delta g(\mathbf{r}) = g_{cryst}(\mathbf{r}) - g_{procryst}(\mathbf{r})$ (*a*) and $\delta v(\mathbf{r}) = v_{cryst}(\mathbf{r}) - v_{procryst}(\mathbf{r})$ (*b*) characterizing the changes in the kinetic and potential energy densities, respectively, caused by the formation of a crystal from the atoms (half of the molecule is shown). Line intervals are 0.02 a.u. Solid lines correspond to excessive (positive) kinetic energy density and (negative) potential energy density.

Thus, kinetic and potential energy distributions reveal details of the stabilizing enhancement in the potential energy and destabilizing increase in the kinetic energy resulting from the formation of crystalline urea. It is remarkable that urea crystallization results in very subtle changes in the *g* and *v* distributions in the hydrogen bond regions (Fig. 7). In agreement with the observation of Spackman (1999), the energy distribution here is close to that in an atomic procrystal. The distributions of *g* and *v* spanning the areas around the ED (3,−1) critical points characterizing the hydrogen bond in urea are very flat. The same observation was recently made by Galvez *et al.* (2001) in their theoretical study of bonding in the hydrogen-bonded dimers. Therefore, quantitative determination of the energy characteristics in the hydrogen bond critical points demands very accurate electron density. Correspondingly, any conclusion that is based on these values should be treated with care.

It is interesting that quasi-classic kinetic energy density $g(\mathbf{r})$ and potential energy density $v(\mathbf{r})$ are structurally homeomorphic to the electron density in LiF and urea. It should be pointed out that, in general, this is not the case (Keith *et al.*, 1996).

4. Concluding remarks

The approach outlined above was tested on rock-salt type crystals (Tsirelson & Ivanov, 2000), perovskites (Zhurova & Tsirelson, 2002), energetic compounds (Zhurova, 2001) and some other crystals with different types of chemical bonds (Tsirelson, 2000). The general conclusion is that this approach may be used at least at the semi-quantitative level for elucidation of the physical nature of atomic and molecular interactions. Moreover, recently we demonstrated that the electron localization function (ELF) can be determined using the Kirzhnits (1957) approximation for kinetic energy density (Tsirelson & Stash, 2002). It possesses all the properties of the quantum-mechanically calculated ELF. This fact gives additional support to the present results.

Note that recently Fuentealba (1997) has suggested an approach to determine the $g(\mathbf{r})$ function using the virial

theorem relationships derived in the density functional theory. Unfortunately, kinetic energy density in this approach depends on the position of origin of the coordinate system: this makes its application to molecules and crystals difficult.

Calculation of all the local energy characteristics from the electron density in this work was performed with the *WinXPRO* program (Stash & Tsirelson, 2002). Multipole parameters were obtained with the aid of the Hansen & Coppens (1978) model using the Clementi & Roetti (1974) wave functions.

References

Abramov, Yu. A. (1997*a*). *Acta Cryst.* A**53**, 264–272.
Abramov, Yu. A. (1997*b*). *J. Phys. Chem.* A**101**, 5725–5728.
Aleksandrov, Yu. V., Tsirelson, V. G., Reznik, I. M. & Ozerov, R. P. (1989). *Phys. Status Solidi B*, **155**, 201–207.
Alonso, J. A. & Girifalco, L. A. (1978). *Phys. Rev. B*, **17**, 3735–3743.
Bader, R. W. F. (1990). *Atoms in Molecules: A Quantum Theory.* Oxford: Clarendon Press.
Bader, R. W. F. (1994). *Phys. Rev. B*, **49**, 13348–13356.
Bader, R. W. F. (1998). *J. Phys. Chem.* A**102**, 7314–7323.
Bader, R. F. W. & Beddall, P. M. (1972). *J. Chem. Phys.* **56**, 3320–3329.
Bader, R. F. W. & Essen, H. J. (1984). *J. Chem. Phys.* **80**, 1943–1960.
Bader, R. F. W. & Platts, J. A. (1997). *J. Chem. Phys.* **107**, 8545–8553.
Bader, R. F. W. & Preston, H. J. T. (1969). *Int. J. Quantum Chem.* **3**, 327–347.
Biegler-Koenig, R. W., Bader, R. F. W. & Tang, T.-H. (1982). *J. Comput. Chem.* **3**, 317–328.
Bone, R. G. A. & Bader, R. F. W. (1996). *J. Phys. Chem.* B**100**, 10892–10911.
Brack, M., Jennings, B. K. & Chu, Y. H. (1976). *Phys. Lett. B*, **65**, 1–4.
Clementi, E. & Roetti, C. (1974). *At. Data Nucl. Data Tables*, **14**, 177–478.
Clinton, W. L., Frishberg, C. A., Goldberg, M. J., Massa, L. Y. & Oldfield, P. A. (1983). *Int. J. Quantum Chem. Symp.* **7**, 505–514.
Cramer, D. & Kraka, E. (1984). *Croat. Chem. Acta*, **57**, 1259–1281.
Dahl, J. P. & Avery, J. (1984). Editors. *Local Density Approximations in Quantum Chemistry and Solid State Physics.* New York: Plenum Press.
Dreizler, R. M. & Gross, E. K. U. (1990). *Density Functional Theory.* Berlin: Springer-Verlag.
Ehrenfest, P. (1927). *Z. Phys.* **45**, 455–460.
Ellis, D. E. (1995). Editor. *Density Functional Theory of Molecules, Clusters and Solids.* Dordrecht: Kluwer.
Espinosa, E. & Molins, E. (2000). *J. Chem. Phys.* **11**, 5686–5694.
Espinosa, E., Lecomte, C. & Molins, E. (1999). *Chem. Phys. Lett.* **300**, 745–748.
Espinosa, E., Molins, E. & Lecomte, C. (1998). *Chem. Phys. Lett.* **285**, 170–173.
Fuentealba, P. (1997). *J. Phys. B*, **30**, 2039–2045.
Galvez, O., Gomez, P. C. & Pacios, L. F. (2001). *Chem. Phys. Lett.* **337**, 263–268.
Gatti, C., Saunders, V. R. & Roetti, C. (1994). *J. Chem. Phys.* **101**, 10686–10694.
Grammaticos, B. & Voros, A. (1979). *Ann. Phys.* **123**, 359–380.
Granovsky, A. (2000). *The PC GAMESS*, http://classic.Chem.msu.su/gran/gamess/index.html.
Gritsenko, O. B. & Zhidomirov, G. M. (1987). *Dokl. Akad. Nauk SSSR*, **293**, 1162–1165.
Hansen, N. & Coppens, P. (1978). *Acta Cryst.* A**34**, 909–921.
Hohenberg, P. & Kohn, W. (1964). *Phys. Rev. B*, **136**, 864–871.
Jayatilaka, D. (1998). *Phys. Rev. Lett.* **80**, 798–801.
Kapphahn, M., Tsirelson, V. G. & Ozerov, R. P. (1988). *Port. Phys.* **19**, 213–216.
Kapphahn, M., Tsirelson, V. G. & Ozerov, R. P. (1989). *Dokl. Phys. Chem.* **303**, 1025–1028.
Keith, T. A., Bader, R. F. W. & Aray, Y. (1996). *Int. J. Quantum Chem.* **57**, 183–198.
Kirzhnits, D. A. (1957). *Sov. Phys. JETP*, **5**, 64–72.
Kirzhnits, D. A., Losovik, Yu. E. & Spatakovskaya, G. V. (1975). *Sov. Phys. Usp.* **18**, 649–672.
Levy, M. & Goldstein, J. A. (1987). *Phys. Rev. B*, **35**, 7887–7890.
Luana, V., Costales, A. & Martin Pendas, A. (1997). *Phys. Rev. B*, **55**, 4285–4297.
Lundqvist, S. & March, N. H. (1983). Editors. *Theory of Inhomogeneous Electron Gas.* New York: Plenum Press.
Martin Pendas, A., Costales, A. & Luana, V. (1998). *J. Phys. Chem.* B**102**, 6937–6948.
Masunov, A. E. & Vyboishchikov, S. F. (1993). *XVI Intern. Crystallogr. Congress. Collect. Abstr.*, p. 380. Beijing.
Parr, R. G. & Yang, W. (1989). *Density-Functional Theory of Atoms and Molecules.* New York: Oxford University Press.
Politzer, P. & Parr, R. G. (1974). *J. Chem. Phys.* **61**, 4258–4262.
Reznik, I. M. (1992). *Electron Density Theory of Ground State Properties of Crystals.* Kiev: Naukova Dumka.
Santos, E. & Villagra, A. (1972). *Phys. Rev. B*, **6**, 3134–3141.
Schmider, H., Edgecombe, K. E., Smith, V. H. & Weyrich, W. (1992). *J. Chem. Phys.* **96**, 8411–8419.
Schmidt, M. W., Baldridge, K. K., Boatz, J. A., Elbert, S. T., Gordon, M. S., Jensen, J. H., Koseki, S., Matsunaga, N., Nguyen, K. A., Su, S. J., Windus, T. L., Dupuis, M. & Montgomery, J. A. (1993). *J. Comput. Chem.* **14**, 1347–1363.
Schwarz, K. W. E & Mueller, B. (1990). *Chem. Phys. Lett.* **166**, 621–626.
Spackman, M. A. (1999). *Chem. Phys. Lett.* **301**, 425–429.
Springborg, M. (1997). Editor. *Density-Functional Method in Chemistry and Materials Science.* Chichester: J. Wiley & Sons.
Stash, A. & Tsirelson, V. (2002). *J. Appl. Cryst.* **35**, 371–373.
Tal, Y. & Bader, R. F. W. (1978). *Int. J. Quantum Chem. Symp.* **12**, 153–168.
Tsirelson, V. G. (1992). *VI Conference on Crystal Chemistry of Inorganic Compounds.* Abstracts, pp. 258–258. L'viv, Ukraine.
Tsirelson, V. G. (1996). *Can. J. Chem.* **74**, 1171–1179.
Tsirelson V. G. (2000). *Russian National Conference on Crystal Chemistry*. Abstracts, pp. 34–34. Chernogolovka: Institute of Problems of Chemical Physics.
Tsirelson, V. G., Abramov, Yu. A., Zavodnik, V. E., Stash, A. I., Belokoneva, E. L., Stahn, J., Pietsch, U. & Fell, D. (1998). *Struct. Chem.* **9**, 249–254.
Tsirelson, V. & Ivanov, Yu. (2000). *Sagamore XIII. Conference on Charge, Spin and Momentum Densities*. Book of Abstracts, p. 104. Byalistok: Institute of Experimental Physics.
Tsirelson, V. G., Mestechkin, M. M. & Ozerov, R. P. (1977). *Dokl. Akad. Nauk*, **233**, 108–110.
Tsirelson, V. G. & Ozerov, R. P. (1979). *Kristallographia*, **24**, 1156–1163.
Tsirelson, V. G. & Ozerov, R. P. (1996). *Electron Density and Bonding in Crystals.* Bristol/Philadelphia: Institute of Physics.
Tsirelson, V. & Stash, A. (2002). *Chem. Phys. Lett.* **351**, 142–148.
Weizsaecker, C. F. (1935). *Z. Phys.* **96**, 431–444.
Yang, W. (1986). *Phys. Rev. A*, **34**, 4575–4585.
Yang, W., Parr, R. G. & Lee, C. (1986). *Phys. Rev. A*, **34**, 4586–4590.
Yang, Z-Z., Liu, S. & Wang, Y. A. (1996). *Chem. Phys. Lett.* **258**, 30–36.
Zavodnik, V. E., Stash, A. I., Tsirelson, V. G., de Vries, R. & Feil, D. (1999). *Acta Cryst.* B**55**, 45–54.
Zhao, Q. & Parr, R. G. (1993). *J. Chem. Phys.* **98**, 543–548.
Zhurova, E. A. (2001). Personal communication.
Zhurova, E. A. & Tsirelson, V. G. (2002). *Acta Cryst.* **58**, 567–575.